

Understanding the nanoscale structure of hexagonal phase lyotropic liquid crystal membranes

Benjamin J. Coscia Douglas L. Gin Richard D. Noble Joe Yelk
Matthew Glaser Xunda Feng Michael R. Shirts

April 30, 2018

Introduction

Nanostructured membrane materials have become increasingly popular for aqueous separations applications such as desalination and biorefinement because they offer the ability to control membrane architecture at the atomic scale allowing the design of solute-specific separation membranes. [1]

- Most membrane-based aqueous separations of small molecules can be achieved using reverse osmosis (RO) or nanofiltration (NF) [2]

While RO and NF have seen many advances in the past few decades, they are far from perfect separation technologies.

- *RO membranes*

- Inconsistent performance : Current state-of-the-art RO membranes are unstructured with tortuous and polydisperse diffusion pathways which leads to inconsistent performance [3]
- High energy requirements : Necessarily high feed pressures drive up energy requirements which strains developing regions and contributes strongly to CO₂ emissions. [4]
- Separation based on differences in solubility and diffusivity: Moreover, designing RO membranes to achieve targeted separations of specific solutes in a complex feed solution is nearly impossible because various solutes dissolve into and diffuse through the polymer matrix at different rates. [5]
- With optimization, one can exploit these differences to create a functional selective barrier.

- *NF membranes*

- NF was introduced as an intermediate between RO and ultrafiltration, having the ability to separate organic matter and salts on the order of one nanometer in size.
- Larger and well-defined pores drive down energy requirements while still affording separation of solutes as small as ions to some degree [2]
- NF is often used as a precursor to reverse osmosis
- Unfortunately, NF membranes, like RO, possess a pore size distribution which limits their ability to perform precise separations [6]

Nanostructured membranes can bypass many of the performance issues which plague traditional NF and RO membranes.

- Tune size and functionality of building blocks to control pore size and shape: One can accomplish targeted separations with high selectivity by tuning shape, size and functionality of the molecular building blocks which form these materials.

- As a result, solute rejecting pores can have their sizes tuned uniformly, resulting in strict size cut-offs.
- Entirely different mechanisms may govern transport in a given nanostructured material which can inspire novel separation techniques.

Development of nanostructured materials has been limited by the ability to synthesize and scale various fundamentally sound technologies.

- Graphene sheets are atomically thick which results in excellent permeability but defects during manufacturing severely impact selectivity. [7]
- Molecular dynamics simulations of carbon nanotubes show promise [1] but synthetic techniques are unable to achieve scalable alignment and pore monodispersity.[8, 9]
- Zeolites have sub-nm pores with a narrow pore size distribution and MD simulations exhibit complete rejection of solvated ions, [10] however, experimental rejection was low and attributed to interstitial defects formed during membrane synthesis [11]
- There is a need for a scalable nanostructured membrane

Self assembling lyotropic liquid crystals (LLCs) are a suitable candidate for aqueous separation applications.

- LLCs share the characteristic ability of nanostructured membrane materials to create highly ordered structures with the added benefits of low cost and synthetic techniques feasible for large scale production [12]
- Neat liquid crystal monomer forms the thermotropic, Col_h phase. The presence of water results in the H_{II} phase.
- In both cases, monomers assemble into mesophases made of hexagonally packed, uniform size, cylinders with hydrophilic groups oriented inward towards the pore center and hydrophobic groups facing outward.
- H_{II} and Col_h phase systems created by the monomer named Na-GA3C11 have been extensively studied experimentally [13, 14, 15, 12, 16].

Research into LLC membranes has been revived in recent years.

- During early stages of exploration, mesophases formed by Na-GA3C11 could not be macroscopically aligned, resulting in low flux membranes, and no clear route towards scalable and economical filtration.
- In 2014, Feng et al. showed that the mesophases could be aligned using a magnetic field with subsequent crosslinking to lock the structure in place [12]
- In 2016, Feng et al. showed that the same result could be obtained using a technique termed soft confinement [16].

A molecular level understanding of LLC membrane structure, enabled by molecular dynamics simulations, will provide guidelines to reduce the large chemical space available to design monomers for creation of separation-specific membranes.

- Over the past 20 years, H_{II} phase LLC membrane studies have been limited primarily to Na-GA3C11 with some characterization done after minor structural modifications
- Resel et al. varied the length of the monomer tails and the counterion used and observed its affect on pore spacing [17].
- Rejection studies show that this membrane can not perform separations of solutes less than 1.2 nm in diameter because the pores are too large [14].

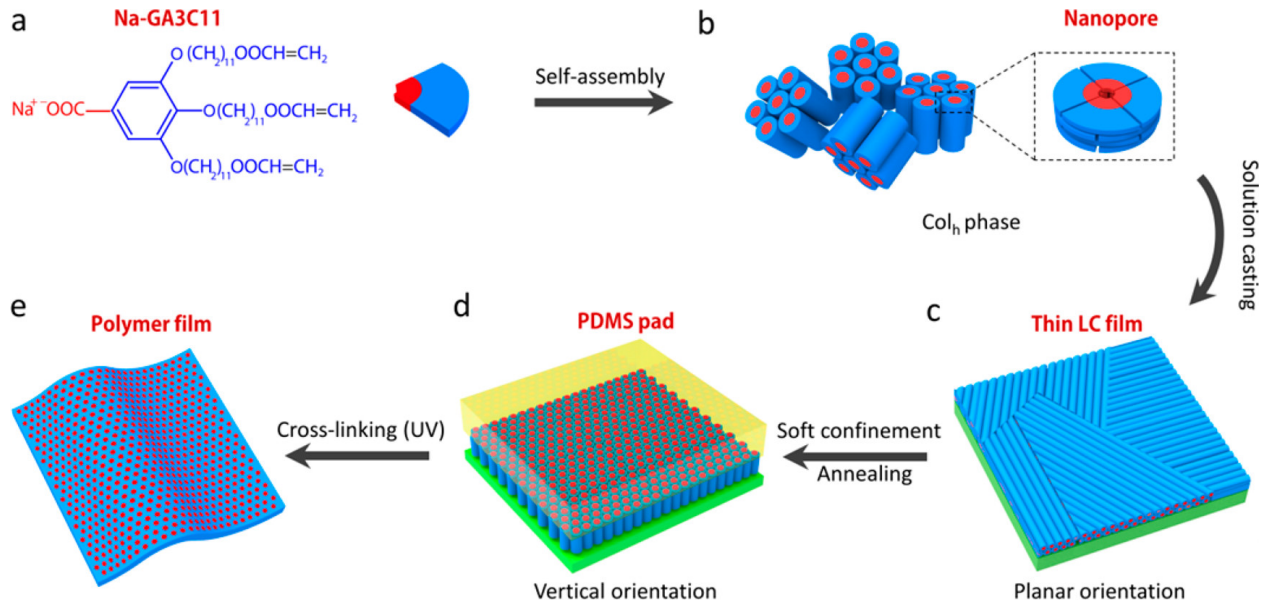


Figure 1: The wedge shaped liquid crystal monomer (a) self assembles into mesophases with hexagonally packed pores (b). The pores are made of stacked monomer disks. A sub-micron-thick film is created by casting a dilute solution of Na-GA3C11/THF solution onto a silicon substrate and allowing the solvent to evaporate. The thin film contains nanoporous columns which lie parallel to the film plane. (d) When a soft PDMS pad is imposed to the thin film, with subsequent thermal annealing, the columns align perpendicular to the film plane. (e) Photo-cross-linking of the aligned film creates a mechanically stable thin film with vertically aligned nanopores

- We do not yet understand how to controllably reduce the effective pore size or how to tune the chemical environment in the nanopores for effective water desalination or small organic molecule separations.
- It will be challenging to efficiently narrow down the large design space in a laboratory setting without a robust model.
- The only source of predictive modeling for LLC systems have been macroscopic models which likely do not adequately describe transport at these length scales.
- The choice of head group may allow us to tune pore size for size exclusion driven separations
- Choice of counterion may influence the establishment of a Donnan potential affecting the degree to which the membrane can exclude charged species.
- A good molecular model should incorporate a detailed picture of the nanoscopic pore structure which will be crucial to understanding the role of monomer structure in membrane design.
- Molecular dynamics simulations will provide the required level of detail

Our approach to constructing a general model will follow the development of a model of a specific LLC membrane with sufficient experimental characterization.

- We have chosen to focus on assemblies formed by Na-GA3C11
- We have also narrowed our scope to the development of a model of the Col_h phase membrane.
- Compared to the H_{II} phase, the Col_h phase is a simpler starting point, due to the absence of water, and has detailed experimental WAXS patterns useful for reconstructing structural data.

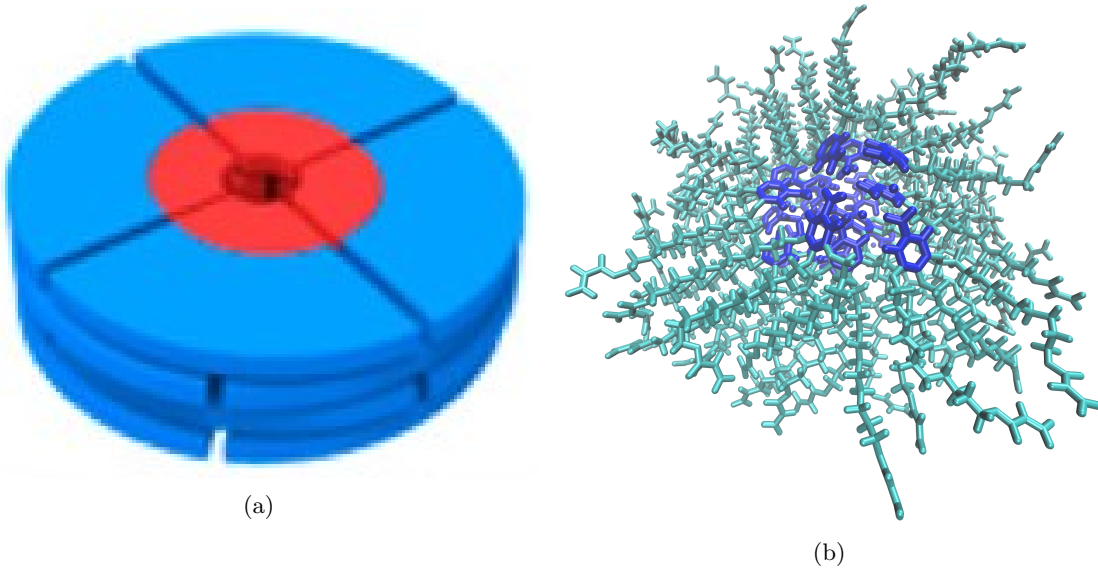


Figure 2: (a) Our previous understanding of the pore structure allows us to speculate about separation behavior. (b) A detailed molecular model will allow us to directly observe solute transport. Here, four stacked layers of 5 monomers are pictured atomistically. The hydrophilic region is in red and the hydrophobic region is colored blue.

Despite having structural data, there is still information which experiment cannot definitively answer. There are several key questions that we will investigate which will be laid out and numbered in subsequent paragraphs.

There are a number of structural questions we wish to answer in this article. We want to know:

1. What is the density of monomers that pack around each hydrophilic core?
 - Authors often describe this and similar systems as being made up of layers.
 - A simple molecular simulation study of a similar molecule suggested that there are 4 monomers in each layer. Their estimation is based on a simulated system containing only 16 total monomers which likely does not sufficiently model the chemical environment present in the real system. [18].
 - A separate calculation based on the volume of the liquid crystal monomers proposes that there are seven monomers in each layer [17].
 - We are careful to avoid the term 'layers' since a liquid crystalline system has, by definition, long range order in 1 or 2 spatial dimensions and short range order in the other dimensions. [?]
 - In the system we are studying, there are long-range 2D correlations in the hexagonal array of pores and short range correlations in the z-direction.
 - We will use our atomistic molecular model to study how the system's structure is effected by the density of monomers surrounding each pore's hydrophilic core.
2. What structural motif best matches experimental 2D WAXS patterns?
 - On the short timescales accessible to MD, we observe distinct metastable configurations which are dependent on starting configuration.
 - We simulate XRD patterns of our system and compare them to experimental 2D WAXS patterns so that we ensure our model creates a nanoscopic chemical environment maximally consistent with experiment within the constraints of our forcefield.

- We are able to confirm and refute previous interpretations of the WAXS pattern.
3. What is the chemical composition of the pores?
- The limited picture that experiment provides tells us that there are hexagonally packed, hydrophilic regions where transport is likely to occur
 - One may instinctively assume that these regions are tube-like pathways with well-defined boundaries.
 - We will explore the composition of the pores, the partition between the hydrophilic and hydrophobic regions, and its sensitivity to initial configuration.
4. Is it necessary to include any water in order to appropriately model the Col_h phase?
- While the Col_h phase is described as dry, it is likely that small amounts of ambient water may be leached into the system.
 - The hydrogen bonding network formed by the water may play a role in structuring the pore.
 - We can use simulated X-ray diffraction patterns to see if there is any meaningful structural difference between a "dry" and "wet" system

In this study, we build a significantly more realistic atomistic model of LLC membranes than has ever previously been done, and explore what new structural information can be gained and what structure hypotheses are supported by this model.

- We validate the model using as much experimental information as possible.
- We are most interested in reproducing the conclusions about structure which have been made from X-ray diffraction (XRD) experiments and in matching ionic conductivity measurements [16].

We used experimental wide angle X-ray scattering (WAXS) data (produced as described in [12]) and small angle X-ray scattering (SAXS) data from [16] to inform our choices of some initial structural parameters (Figure 3). We rely primarily on the 2D WAXS data since it encodes all structural details down to the sub-nm scale.

- There are five major features of interest present in the 2D experimental pattern shown in Figure 3b.
- The first is located at $q_z = 1.7 \text{ \AA}^{-1}$, corresponding to a real spacing of 3.7 \AA . The reflection is attributed to $\pi-\pi$ stacking between aromatic rings in the direction perpendicular to the membrane plane, or z-axis [12]. For simplicity, this reflection will be referred to as R- π .
- A weak intensity line is located at exactly half the q_z value of R- π ($q_z = 0.85 \text{ \AA}^{-1}$), corresponding to a real space periodic spacing of 7.4 \AA . This reflection has been interpreted as 2_1 helical ordering of aromatic rings along the z axis meaning if the positions of the aromatic rings can be traced by a helix, then for each turn in the helix, there should be two aromatic rings. For this reason it will be referred to as R-double.
- A third major reflection is marked by a low intensity ring located at $r = 1.4 \text{ \AA}^{-1}$. The real space separation corresponds to 4.5 \AA which is characteristic of the average spacing between packed alkane chains. This reflection will be called R-alkanes.
- Within R-alkanes, are four spots of higher relative intensity which will be called R-spots. All are located ≈ 40 degrees from the q_z axis in their respective quadrants. In many liquid crystal systems this can be explained by the tilt angle of the alkane chains with respect to the xy plane.
- The final feature corresponds to the spacing and symmetry of the d_{100} plane which can be related to the distance between pores. The feature, which will be called R-pores, is characterized by dots along $q_z = 0$. The spacing between dots is indicative of the hexagonal symmetry of the packed pores. The same information at higher resolution is obtained using a SAXS setup. By radially integrating the 2D data one gets a 1D curve which is shown in Figure 3a.

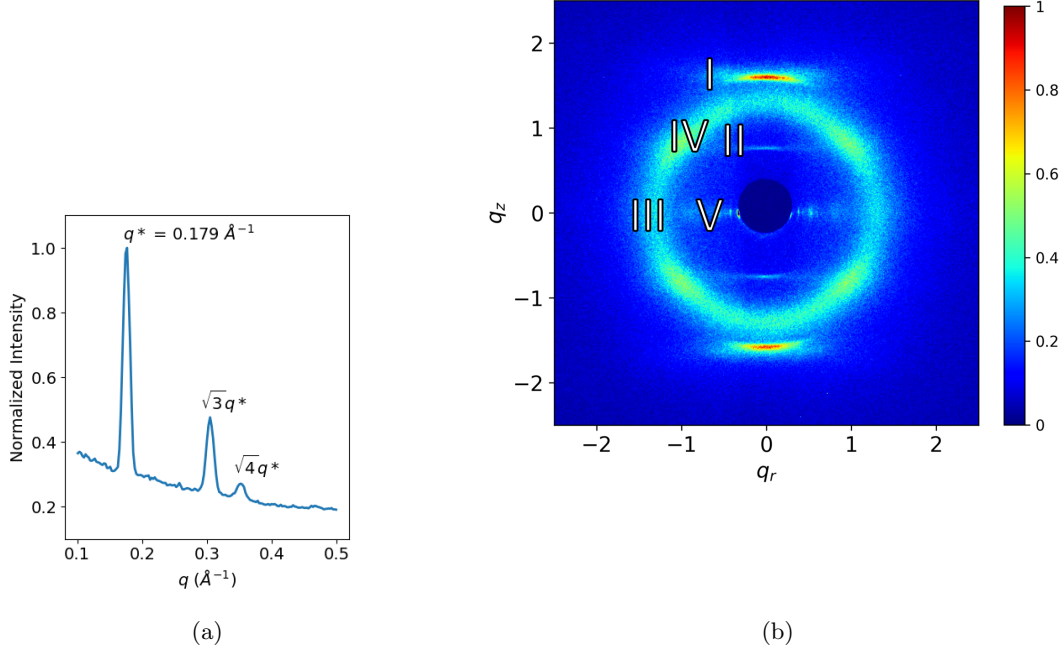


Figure 3: (a) 1D small angle X-ray scattering indicates hexagonal packing of pores as well as the spacing between pores (b) 2D wide angle X-ray scattering gives details about repeating features less than 1 nanometer apart

Methods

Liquid crystal monomers were parameterized using the Generalized AMBER Forcefield [23] with the Antechamber package [24] provided with AmberTools16 [25]. Atomic charges were assigned using the am1bccsym method of molcharge shipped with QUACCPAC from Openeye Scientific Software. All molecular dynamics simulations were run using Gromacs 2016 [26, 27, 28, 29]

An ensemble of characteristic, low-energy vacuum monomer configurations were constructed by applying a simulated annealing process to a parameterized monomer.

- Monomers were cooled from 1000K to 50K over 10 nanoseconds.
- A low energy configuration was randomly pulled from the trajectory and charges were reassigned with molcharge.
- Using the new charges, the monomer system was annealed again and monomer configurations were pulled from the trajectory to be used for full system construction (Figure 4a).

The timescale for self assembly of monomers into the hexagonal phase is unknown and likely outside of a reasonable length for an atomistic simulation, calling for a more efficient way to build the system.

- Previous work has shown a coarse grain model self assemble into the H_{II} phase configuration in ≈ 1000 ns [30].
- We attempted atomistic self-assembly by packing monomers into a box using Packmol [31].
- Simulations of greater than 100 ns show no indicators of progress towards an ordered system.
- To bypass the slow self-assembly process, python scripts are used to assemble monomers into a structure close to one of a number of hypothesized equilibrium configurations (Figure 4).

A typical simulation volume contains four pores in a monoclinic unit cell, the smallest unit cell that maintains hexagonal symmetry when extended periodically.

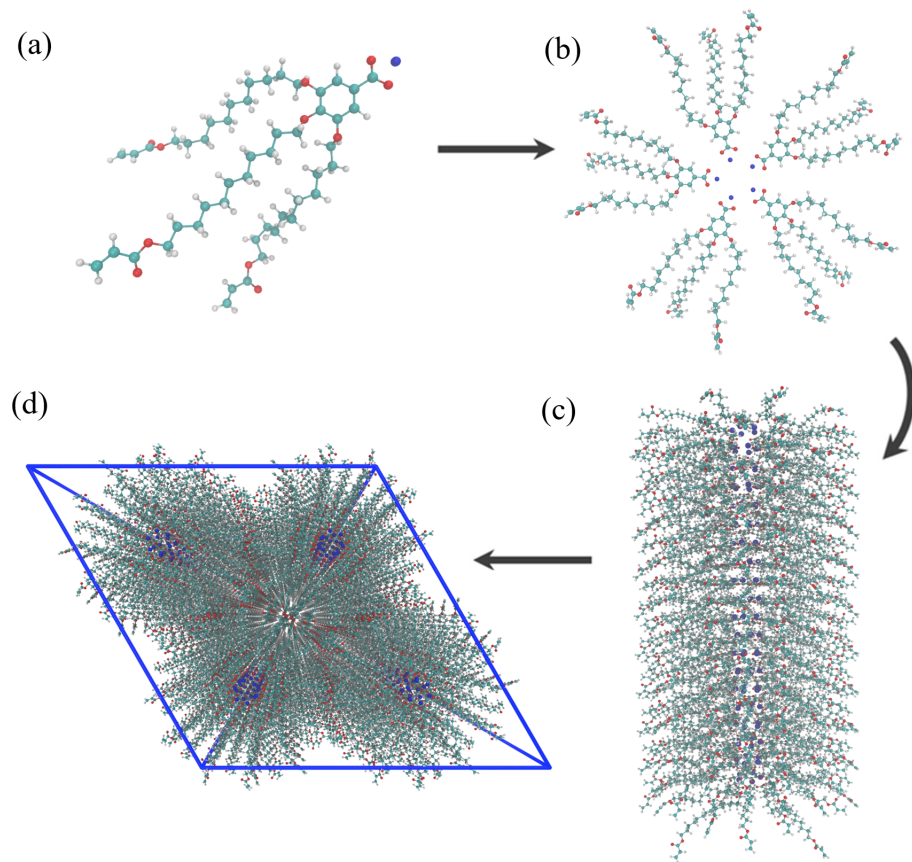


Figure 4: (a) A single monomer was parameterized and annealed to produce a low energy configuration. (b) Monomers are rotated and assembled into layers with hydrophilic centers. (c) Twenty layers are stacked on top of each other to create a pore. (d) Pores are duplicated and placed into a monoclinic unit cell

- Each pore is made of twenty stacked monomer layers with periodic continuity in the z direction, avoiding any edge effects and creating an infinite length pore ideal for studying transport.
- A small number of layers is preferred in order to reduce computational cost and to allow us to look at longer timescales.
- Ultimately, we chose to build a system with 20 monomer layers in each pore in order to obtain sufficient resolution when simulating X-ray diffraction patterns. This point will be explained in more detail later.

When constructing an initial configuration, there are a number of variables which require careful consideration while placing monomers. The equilibrium configuration is sensitive to some while insensitive to others.

- The starting pore radius, defined as the distance of a chosen head group carbon from the pore's central axis, does not influence the equilibrium structure when a reasonable value is chosen (See Supplemental)
- The pore radius is chosen to be 0.6 nm in our initial configurations because the pore size is estimated to be ≈ 1.2 nm
- The initial distance between pores also has little effect on the equilibrated structure. However, one should not start them too close or there will likely be unintended high energy repulsions during early equilibration
- We chose an initial pore spacing of 4.5 nm, $\approx 10\%$ larger than the experimental value of 4.12 nm.
- The distance between layers and the rotation of the layers with respect to adjacent layers, and the number of monomers per layer do influence the equilibrium structure and require further justification for their choices.
- We rely on experimental data to inform our choices

We chose the layer spacing for the initial configuration based on $R-\pi$ and then allowed system to readjust during equilibration.

- Each monomer was rotated so the plane of the aromatic head groups would be coplanar with the xy plane.
- We explore two different initial layer spacings
- The first is exactly equal to $R-\pi$ with layers placed so aromatic rings are stacked 3.7 Å apart in the z-direction.
- A second system is explored with an initial layer spacing of 5 Å
- A third system with an initial layer spacing of 10 Å was briefly explored
- When layers are spaced out sufficiently, they tend to collapse on each other while simultaneously slipping in between layers of other pores which lead to an artificially thick membrane with pores spaced closely together.
- The interested reader can learn more about it in the Supplemental Information.

The relative interlayer orientation was chosen based on clues from diffraction data as well as the various known stacking modes of benzene and substituted benzene rings: sandwiched, parallel-displaced and T-shaped [20] (Figures 5a to 5c).

- The T-shaped configuration was ruled out based on the inconsistency of its ≈ 5 Å equilibrium stacking distance [20].
- The system's preference towards the sandwiched vs. parallel displaced stacking modes will be explored.
- Both have reported stacking distances near the $R-\pi$ value of 3.7 Å

- Headgroups in our sandwiched initial configuration are stacked directly on top of each other while stacked headgroups in the parallel displaced initial configuration are offset by $180/nmon$ degrees where $nmon$ equals the number of monomers per layer.

As outlined in 1 the number of monomers in each layer is unknown so we tested configurations constructed with a varied number of monomers per layer.

- Systems were built in the offset and parallel displaced configurations with 4, 5, 6, 7 and 8 monomers per layer

We developed equilibration schemes to create dry and wet configurations. Both schemes start with an initial configuration generated according to the previous guidelines.

- Dry equilibration scheme:

- Restraints with a force constant of $1e6 \text{ KJ mol}^{-1} \text{ nm}^{-2}$, fix monomer head groups in the sandwiched or parallel-displaced configurations while allowing monomer tails to settle.
- Doing so also mitigates system dependence on initial monomer configuration.
- The restrained portion of the equilibration scheme is run in the NVT ensemble.
- Every 50 ps, we reduce the force constants by the square root of its previous value
- Once the force constant is below $10 \text{ KJ mol}^{-1} \text{ nm}^{-2}$, the restraints are released linearly until there is no more restraining potential.
- The resulting unrestrained structure is allowed to equilibrate for 5 ns in the NPT ensemble with pressure controlled by the berendsen barostat.
- Long, NPT equilibration simulations are run for at least 400 ns using the Parrinello-Rahman barostat with a time constant of 10 ps.

- Wet equilibration scheme:

- In order to create a wet system, we solvated an initial configuration with water using gmx solvate
- All water molecules placed outside the pore region are removed
- Waters inside the pore region are randomly removed until the desired concentration of water in the pores is reached.
- The remainder of the equilibration is the same as the dry system

- In all cases, the v-rescale thermostat was used with $\tau_{\text{au-t}} = 0.1$

Using an equilibrated structure, a crosslinking procedure was performed in order to match synthetic procedures.

- The purpose of crosslinking is to maintain macroscopic alignment of the crystalline domains, ensuring aligned, hexagonally packed pores.
- For that reason, we are not concerned with replicating the kinetics of the reaction, but instead emphasize the consistency of the final structure with experimental structural data.
- The algorithm was developed based on the known reaction mechanism.
- Crosslinking of this system is a free radical polymerization (FRP) taking place between terminal vinyl groups present on each of the three monomer tails.
- FRPs require an initiator which bonds to the system, meaning new atoms were introduced into the system.
- For simplicity, the initiator was simulated as hydrogen and made present in the simulation by including them in all possible bonding positions as dummy atoms.

- The crosslinking procedure is carried out iteratively.
- During each iteration, bonding carbon atoms are chosen based on a distance cut-off.
- The topology is updated with new bonds and dummy hydrogen atoms are changed to appropriate hydrogen types.
- Head-to-tail addition was the only propagation mode considered due to its dominance in the real system.
- Direction of attack was not considered because the resultant mixture is racemic.

Using equilibrated structures, we carry out various calculations to characterize the system.

- We determine the point at which a system is equilibrated when the distance between pores stops changing

To calculate the equilibrated pore spacing, we measured the distance between pore centers.

- Pore centers were located by averaging the coordinates of sodium ions in their respective pores.
- Statistics were generated using the bootstrapping technique (See Supplemental Information)
 - We are interested in 5 pore-to-pore distances which should all be equal in a perfect hexagonal array, however only 4 distances are independent
 - Each pore spacing has its own trajectory of spacing vs. time. Using data collected after the system is equilibrated, we calculate how long it takes for the data in each of the 5 trajectories to become uncorrelated using `pymbar.timeseries.integratedAutocorrelationTime()`
 - We break the full trajectories down into sub-trajectories based on the maximum autocorrelation time of those found in the previous step.
 - For each bootstrap trial, we recreate an equilibrium trajectory by randomly sampling pore spacings from the sub-trajectories
 - We get an average value for each pore spacing by finding the mean of the bootstrapped data
 - We calculate the overall average as the mean of all bootstrapped pore spacings
 - The uncertainty for each pore spacing is calculated as $\frac{\langle x \rangle - x}{4}$ where $\langle x \rangle$ is the average spacing from the bootstrap trial and x is the average value of one of the pore spacings.
 - We report the mean of these uncertainties

To quantify the degree of layering and the equilibrium distance between layers in our system, we calculate a spatial correlation function, $g(z)$, measured along the z-axis (perpendicular to the membrane plane).

- To calculate $g(z)$, we binned the z component distances between the center of mass of each component and all others of the same pore over at least 50 ns of equilibrated trajectory and then normalized by the average number density.
- To extract the average distance between layers we applied a discrete fourier transform to $g(z)$ and extracted the highest intensity frequency

Simulated X-ray diffraction patterns were generated based on atomic coordinates for a direct experimental comparison.

- All atomic coordinates were simulated as gaussian spheres of electron density corresponding to each atom's atomic number.
- A three dimensional fourier transform (FT) of the array of electron density results in a three dimensional structure factor which represents the unit cell in reciprocal space. z axis to generate a 2D cross section close to what one would see experimentally.

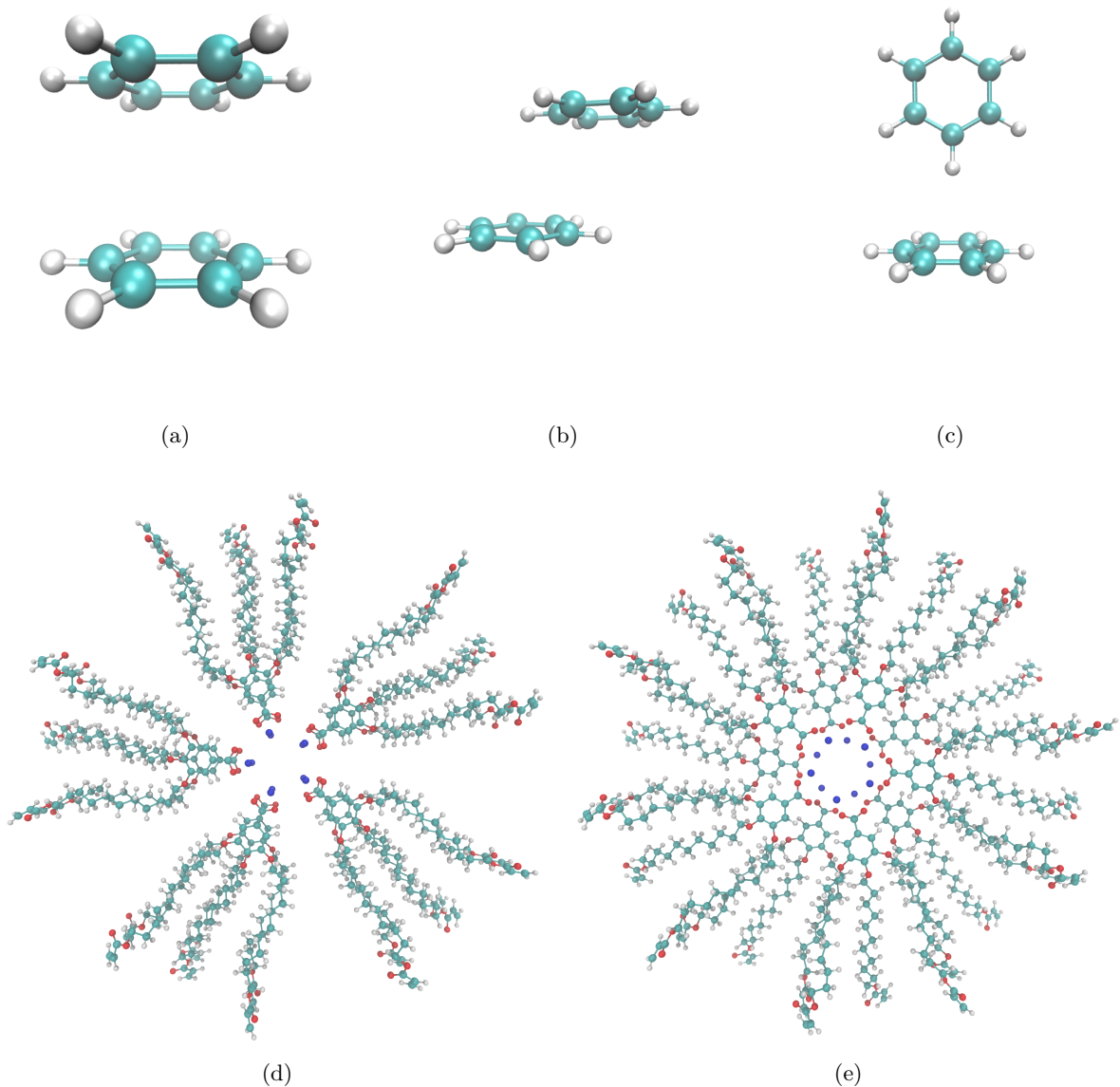


Figure 5: (a) Sandwiched benzene dimers stack 3.8 Å apart. (b) Parallel-Displaced benzene dimers stack 3.4 Å vertically and 1.6 Å horizontally apart. (c) T-shaped benzene dimers stack 5.0 Å apart. (d) Two monomer layers stacked in the sandwiched configuration (e) Two monomer layers stacked in the parallel-displaced configuration

- We matched experimental 2D WAXS patterns by adjusting the initial spacing between layers and the orientation of the head groups with respect to adjacent layers.

We explored the pore composition by measuring the average number densities of various monomer components with respect to the pore centers.

- The centers of the pores were located using the same method to calculate the equilibrium pore spacing
- We looked at the average number density of sodium ions, aromatic rings and carbon atoms making up the monomer tails
- The radial distance from the pore center of all atoms in each group are binned then normalized by area

We calculated ionic conductivity using two different methods for robustness.

- The Nernst-Einstein relation relates the DC ionic conductivity to ion diffusivity, D , concentration, C , ion charge, q , the boltzmann constant, k_b , and temperature, T :

$$\sigma = \frac{q^2 C D}{k_b T}$$

- Sodium ion diffusion coefficients were found by calculating the slope of the linear region of the z-direction mean square displacement curve as indicated by the einstein relation [32].]
- We looked at the MSD plot to determine where to begin and end a linear fit
- Ion concentration was measured with respect to the entire unit cell.
- The second method, termed the 'Collective Diffusion' model, measures the movement of the collective variable, Q , which is defined as the amount of charge transfer through the system and can be thought to represent the center of charge of the system.
- The conductance, γ of the system can be calculated as:

$$\gamma = \frac{D_Q}{k_b T}$$

Conversion to ionic conductivity is achieved by multiplying by channel length and dividing by the membrane cross sectional area.

- D_Q is the diffusion coefficient of the collective variable Q . It can be calculated using the einstein relation.
- A full derivation of the model can be accessed elsewhere [33].

Results and Discussion

0.1 Density of monomers around pores

Our simulations best support a model built with 5 monomers per layer based on the measured equilibrated pore-to-pore distances. To discern the composition of the monomer layers, addressing question (1), we ran simulations of systems created with 4–8 monomers per layer.

- We built systems in both the parallel displaced and sandwiched configurations and equilibrated them according to the dry equilibration procedure.
- We test all systems with an initial layer spacing, l , of 3.7 Å.
- We tested 4 additional systems with layers initially spaced 5 Å apart (See supporting info for more details on sensitivity to initial layer spacing)

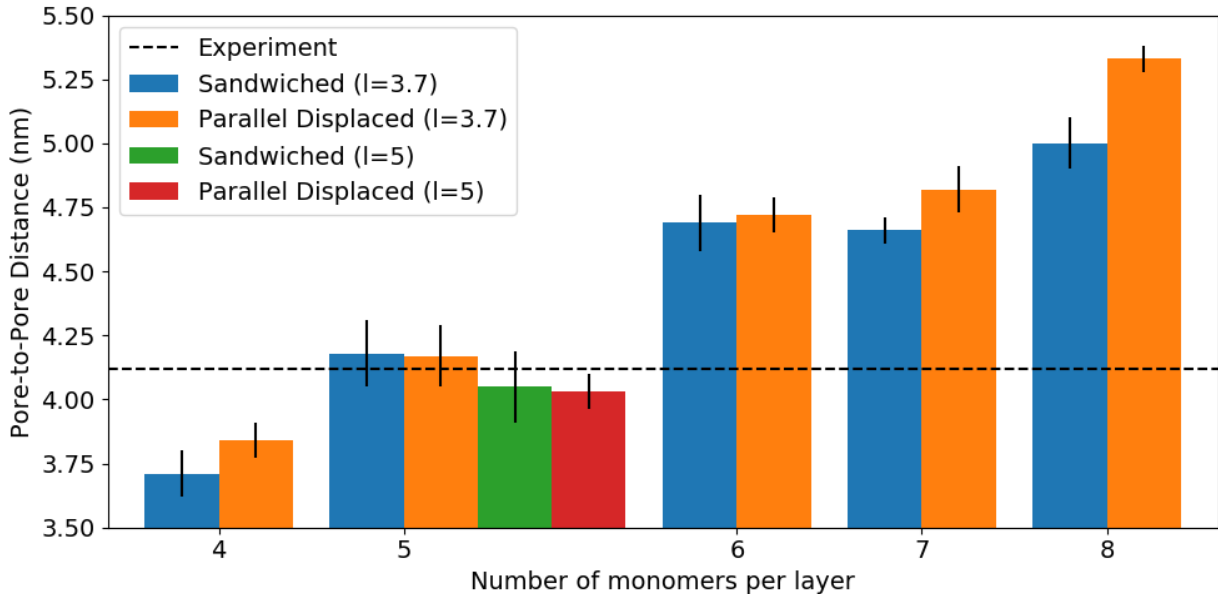


Figure 6: Systems with 5 monomers per layer have equilibrated pore spacings closest to the experimental value of 4.12 nm, regardless of initial layer spacing, l . The equilibrated pore spacing of the model increases as the number of monomers in each layer increases. The pore spacing of systems starting in the sandwiched configuration are systematically lower than those started in the parallel displaced configuration.

- The pore-to-pore spacing is stable in all systems after 400 ns of simulation. Figure 6 shows the equilibrated pore-to-pore distances for all systems tested.
- Systems built with 5 monomers in each layer equilibrate to a pore spacing that is most consistent with the experimental value of 4.12 nm derived from SAXS measurements (Figure 3a).
- comment about disordered systems

The remainder of this discussion will focus on the analysis of systems built with 5 monomers per layer.

- Systems built with 6 monomers per layer have an equilibrated pore spacing c.a. 0.50 nm higher than experiment.
- Systems built with 4 monomers per layer equilibrate to a pore spacing 0.25 nm lower than experiment.
- In a sense, all systems tested are at least metastable, however not all will make physical sense or fit the experimental profile that we are trying to match.
- In the limit of infinite simulation time, all simulations will converge to a single density.
- It is our intention to choose an initial configuration which quickly reaches a monomer density close to experiment.

0.2 Structural determination

We further refined our structural understanding of the system by simulating X-ray diffraction patterns produced from equilibrated MD trajectories and comparing them to experiment.

- We tested systems built with 5 monomers per layer in the parallel displaced and sandwiched configurations at 300 K with layers initially spaced 3.7 Å and 5.0 Å apart.

- We generated simulated patterns using portions of simulation trajectory after equilibration.
- The patterns for all structures are shown and compared to experiment in Figure 7.

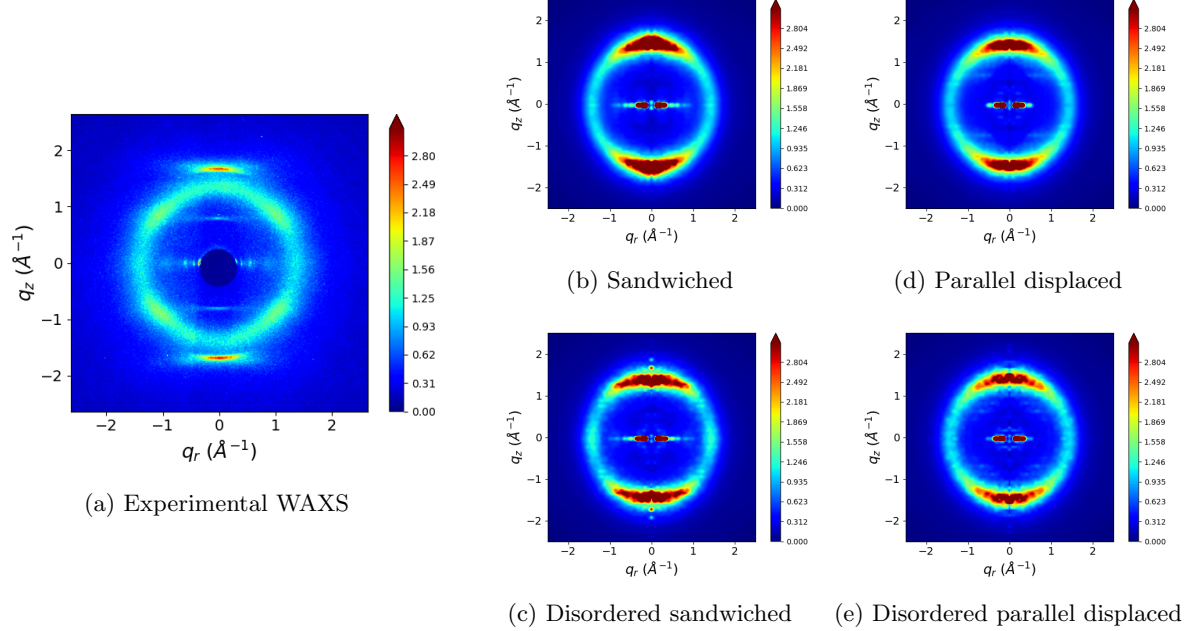


Figure 7: Very descriptive caption

The simulated XRD patterns produced from both systems show moderate qualitative agreement with experiment.

- R-alkanes and R-pores appear in the expected location
- R-pores is more intense than experiment, likely because we are simulating a perfect, infinite hexagonal array. The real system has defects and domain misalignment which decreases the overall intensity.
- R-spots appears to be weaker in the simulated patterns. They are also partially engulfed by the wide R- π reflection.
- We further explore R-spots in Section 0.2.1
- R- π appears at a lower q_z value than experiment. In all systems, the reflection reaches its maximum at $q_z < 1.5 \text{ \AA}^{-1}$ which means that monomers prefer stack greater than 4.2 Å apart rather than 3.7 Å. This behavior is not surprising since GAFF models atoms as point charges and does not appropriately model the aromatic $\pi - \pi$ interactions which would cause the monomers to stack closer together.
- We will explore R- π in more detail in Section 0.2.2.
- R-double does not appear in any of the patterns
- We will explore its possible origins and reasons that it does not appear in our simulated patterns in Section 0.2.3.

The simulated XRD pattern of the parallel displaced configuration shows an additional reflection due to its helical structure.

- There are horizontal reflections at $|q_z| = 0.7 \text{ \AA}^{-1}$, exactly half of the q_z value of R- π .

- The reflection does not cross through $q_r = 0 \text{ \AA}^{-1}$ so it does not appear for the same reason as R-double.
- This type of pattern is characteristic of a helix (reference something)
- It is possible that these reflections contribute to the continuation of R-double into R-alkanes, as seen in the experimental pattern.

We quantified the numerical discrepancies present when comparing the relative intensities of each reflection of interest between experimental and simulated patterns.

- Table 1 quantifies the relative intensity of each reflection for each system tested.
- The patterns are normalized so that the average intensity of R-alkanes equals 1.
- We measured the approximate intensity of R- π by measuring the intensity of the peak of the cross-section at $q_r = 0$.
- The relative intensity of R- π is significantly higher than experiment in our simulations.
- R-spots is measured as the average intensity within the region bounded by a 'spot'. Spots are identified based on visual inspection. If there is no easily discernable spot, then the intensity is taken as that of the intersection of R-alkanes at half the q_z value of R- π , since that is where it appears experimentally.
- The intensity of R-spots is slightly lower than experiment in all cases.
- There is no R-double intensity to be measured.

Reflection	Configuration								
	Experiment	Sandwiched	Parallel	Displaced	Disordered	Sandwiched	Disordered	Parallel	Displaced
R-alkanes	1.0	1.0	1.0	1.0	1.0	1.0	1.0	1.0	1.0
R-spots	1.3	1.2	1.2	1.2	1.2	1.2	1.2	1.2	1.2
R- π	2.8	18.1	14.2	14.2	7.8	7.8	7.8	10.0	10.0
R-double	0.9	—	—	—	—	—	—	—	—

Table 1: The simulated XRD patterns of the systems tested, normalized so that the average intensity of R-alkanes equals 1, show R- π reflections that are significantly higher than experiment and R-spots reflections that are slightly lower than experiment. R-double does not appear in any patterns, and thus has no measurable intensity.

There are clear differences between our simulated results and experimental results that must be addressed and justified. We will explore the origin of each experimental reflection and form structural hypotheses related to their appearance in our simulated patterns. Specifically, we want answer:

1. What is the origin of R-spots?
2. Why is the intensity of R- π so much greater than experiment?
3. What is the origin of R-double?

0.2.1 Origin of R-spots

We observe an increase in the intensity of R-spots when we simulate systems at 280K.

- R-spots is most intense in the sandwiched configuration (Figure 8b).
- The relative intensity of R-spots is higher than in experiment (1.5 vs. 1.3)
- Still no R-double

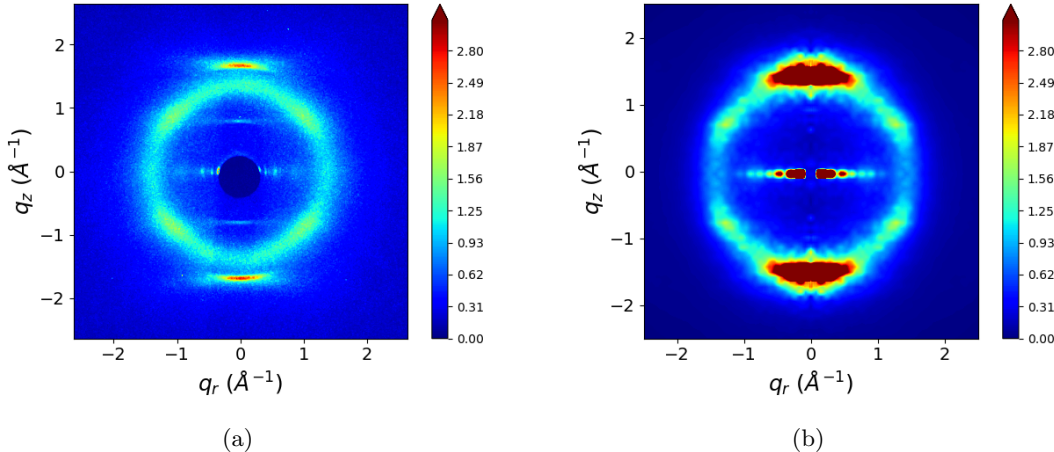


Figure 8: R-spots increases in intensity when the temperature of the system is lowered to 280K. In this case, the simulated R-spots is more intense than experiment.

- We can use this configuration to more thoroughly explore the origin of R-spots.

The R-spots signal is not a result of alkane chain tilt. Previous literature has attributed the spots in this particular WAXS pattern as the product of tilted alkane chains [12]. We looked closer at the sandwiched configuration simulated at 280K since R-spots appears with the most strength in its simulated XRD pattern. We measured the tilt angle of the alkane chains and showed that our system equilibrates to an average tilt angle close to zero degrees (Fig. 9).

To understand the origin of R-spots, we determined which atoms gave rise to the feature. Since R-spots is present as higher intensity spots within R-alkanes, it is likely that the spots arise as a consequence of the tails. By removing all non-tail atoms from the trajectory and simulating a diffraction pattern with the remaining atoms, we were able to isolate the cause of the spots to the tails (Figure 10). Since the tails stay nearly flat, we plotted the centroids of the tails and measured the angle between each centroid and its nearest neighbors with respect to the plane of the membrane. We see distinct peaks in the distribution of these angles (Figure 11).

The peaks in the nearest neighbor angle distribution are consistent with the location of R-spots. The peaks of interest in Figure 11a are located at $\pm 33^\circ$ which is the same location where the highest intensity of spots are located on the simulated patterns. We confirmed this conclusion by radially integrating the 2D WAXS pattern for $|\mathbf{q}|$ values between 1.4 and 1.57 (between 4 and 4.5 Å in real space). We observe that distinct peaks appear c.a. 30° , in close agreement with the previously measured angle distribution (Figure 11b). We performed the same integration on the raw experimental data and found the angle at which R-spots reaches its highest intensity to be $\pm 37^\circ$ which is a reconcilable difference with our simulated results.

There are a couple reasons why we see stronger ordered chain packing at 280 K compared to experimental conditions of 300 K.

1. The difference between 280K and 300K is small. Our forcefield parameters may not correctly model the behavior of the tails at 300K (citation?).
2. Monomers aren't as confined at 300 K in our simulations versus experiment. If the head groups packed 3.7 Å apart, the tails would be more confined and forced to pack between vertically adjacent monomer tails. In our case, the tail region is less dense than experiment which gives the tails freedom to organize in a more entropically favored disordered state.

0.2.2 Discrepancies between R- π

We plotted the one-dimensional pair distribution function, $g(z)$, for the centers of mass of monomer phenyl rings (Figure 12).

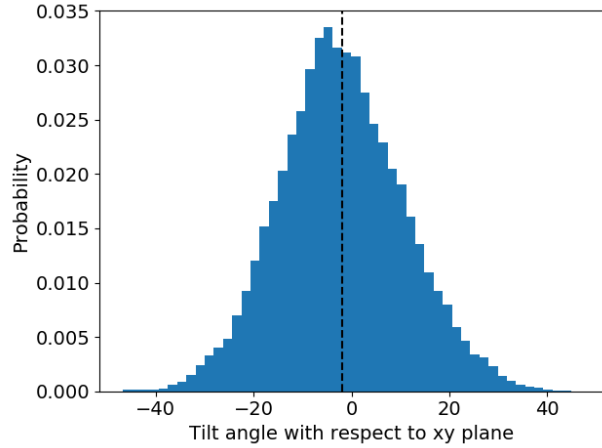


Figure 9: We measured the angle made between each monomer alkane tail and the membrane plane. The average tilt angle (dashed line) is near -2° which is far from the 37° tilt angle previously used to explain R-spots.

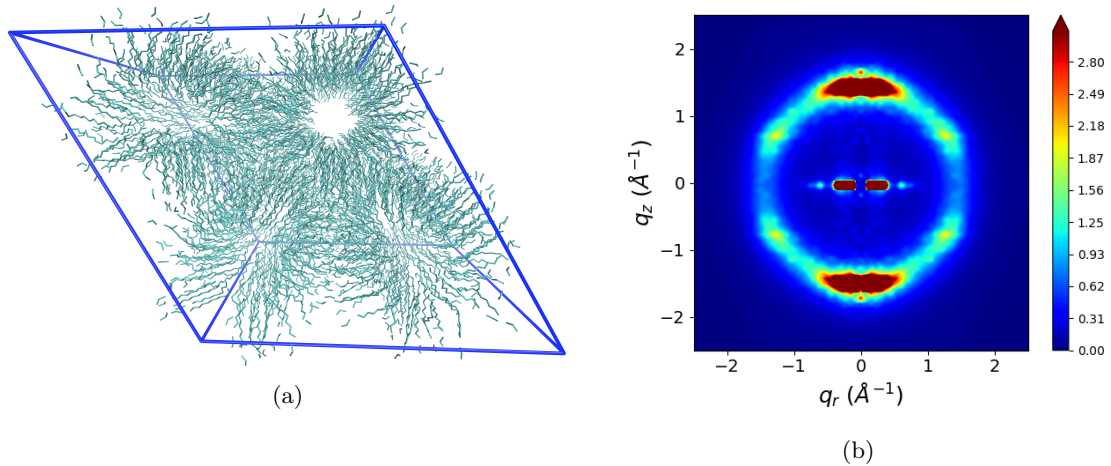


Figure 10: (a) We removed all atoms except carbon atoms that constitute the tails from a sandwiched configuration trajectory. (b) The simulated XRD pattern of the tail-only trajectory still shows R-spots

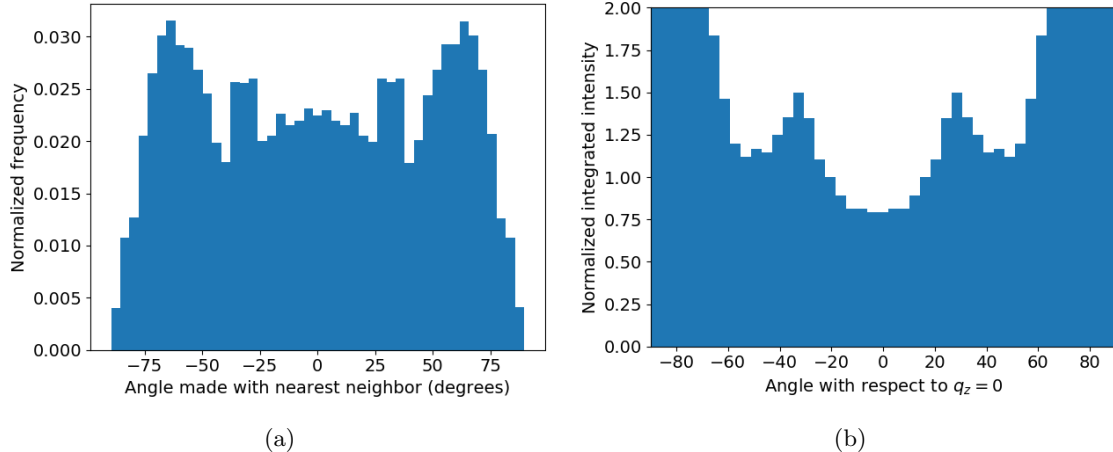


Figure 11: We hypothesize that R-spots is the result of ordered tail packing. Defining the membrane plane to be 0° , we measured the angles between each alkane chain tail centroid and its nearest neighbor centroids for the equilibrated sandwiched configuration simulated at 280K. Peaks that appear in each distribution are centered near $\pm 33^\circ$. We radially integrated the simulated XRD patterns of the parallel displaced and sandwiched configuration within the region bounding R-alkanes. Peaks appear in the same location as the angle distributions which corroborates our hypothesis.

- We averaged all 1D slices in the z-direction of the full 3D correlation function within 2.1 \AA of $(x, y) = (0, 0)$. (full description will be in methods)
- We chose 2.1 \AA as a crude approximation of the radius of the phenyl ring plane.
- We calculated it as the sum of the longest C-C distance within a phenyl ring (2.8 \AA) and two times the carbon atom radius (0.7 \AA).

The correlation length between stacked monomer head groups shows the best agreement with experimental for systems simulated in the ordered basin.

- Correlation length was calculated by fitting a decaying exponential function to all peaks of $g(z)$ for the sandwiched configuration and to every other peak of $g(z)$ for the parallel displaced configuration.
- The correlation length of systems simulated in the ordered basin were 11.2 \AA and 14.9 \AA for the parallel displaced and sandwiched configurations respectively.
- Something about disordered systems.
- Systems simulated in the ordered basin show correlation closest to the experimental correlation length of 10.1 \AA . They are still slightly more correlated than experiment which would lead to an increase in constructive X-ray scattering.

Additionally, our system models near-perfectly straight pores with no defects which will lead to higher intensity vertical stacking reflections.

- Nearly all of the intensity in $R-\pi$ of our simulated patterns is concentrated at a single point. Figure 13 shows the same simulated patterns with the upper boundary on the colorbar adjusted to be 6x higher. The only distinguishable reflections are those of $R-\pi$ and $R\text{-pores}$.
- In the experimental pattern, the intensity is more evenly spread out over all of $R-\pi$.

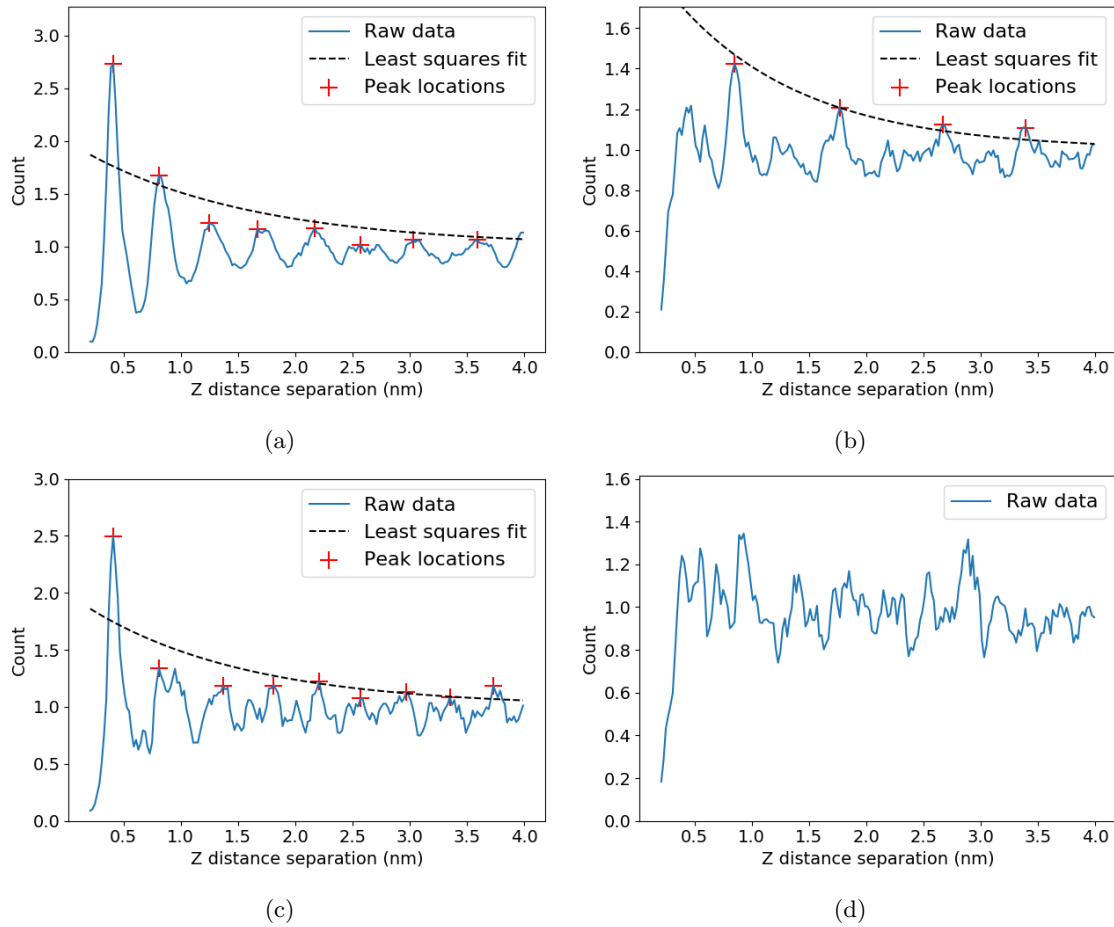


Figure 12

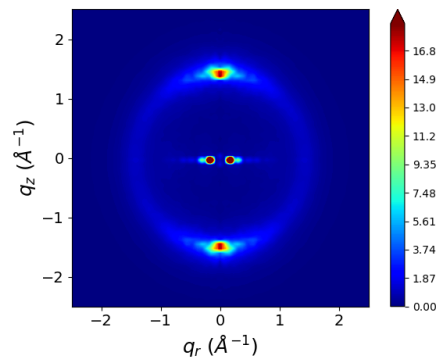


Figure 13: R- π and R-pores are far more intense than the other major reflections. Here, the colorbar was scaled so that the max is 6x higher than all other plots.

0.2.3 Origin of R-double

R-double will not show up in any of the models tested so far.

- All monomers used to build initial configurations are identical. There is no way to produce R-double without a more complex initial configuration
- We calculated the structure factor of simple systems that mimic the parallel displaced and sandwiched configurations. Neither give rise to R-double. (See Figure "fourier transforms of simple systems").
- The reflection implies a vertical modulation in electron density every 7.4 Å.
- This modulation can occur in either the head or the tails
- There is not a unique solution to this problem, however we can speculate based on what makes the most physical sense.

We can produce R-double if our initial configuration contains alternating parallel and antiparallel carboxylate groups relative to the plane of the monomer's phenyl ring. (Figure 14a).

- It is difficult to physically justify this system.
- Systems built this way are only stable if position restraints are placed on all head group heavy atoms. Carboxylate groups quickly revert to the parallel position as restraints are released.
- There is an appreciable energy barrier that prevents rotation of carboxylate groups attached to phenyl rings since the group extends the system's π conjugation. (citation) (See figure in supporting info with energy barrier plots)
- There are instances where carboxylate groups in other systems rotate out of plane.
- Bushey et al. showed that bulky carbonyl-containing substituents of stacked arene molecules tended to tilt 45° in order to relieve steric strain, thus allowing π -stacking between molecules, and to hydrogen bond with neighboring molecules.
- Lorenzo and Graña found 3 stable dimers of gallic acid (from which the monomer, NA-GA3C11 was derived) with adenine. In all cases, the carboxylate group remained planar, even with evidence of hydrogen bonding between the carboxyl group and nitrogen atoms of adenine.
- The monomers which we are studying have no opportunities to hydrogen bond and are confined so that any rotation about the phenyl-carboxylate bond would be sterically hindered.

We can also produce R-double if layers are not uniformly spaced. Rather, monomers might form pairs that stack less than 3.7 Å apart, and whose center of masses are spaced 7.4 Å from the next pair of monomers. (Figure 14b)

- To our knowledge, there have been no studies that specifically address the possibility of a configuration like this.
- Our forcefield causes our system to tend towards uniformly spaced layers.
- As expected, simulations of this type of system are only stable if position restraints are applied to heavy atoms of the phenyl rings.

Our final hypothesized configuration which produces R-double focus on the orientation of the tails.

- In this configuration, monomers are rotated so that the vector created by the bond extending from the carboxylate carbon to the phenyl ring is oriented $\pm 15^\circ$ with respect to the vector extending from the carboxylate carbon to the pore center (Figure 14c)
- Every other monomer layer is rotated $+15^\circ$ and those in between are rotated -15° .

- This configuration allows monomer tails to sit between adjacent monomer tails which may be the most favorable way for them to pack.
- This configuration is stable short-term while unrestrained.
- This may be the most reasonable explanation for the appearance of R-double. The long-term stability of a configuration similar to this may be feasible if monomers stay stacked 3.7 Å apart.

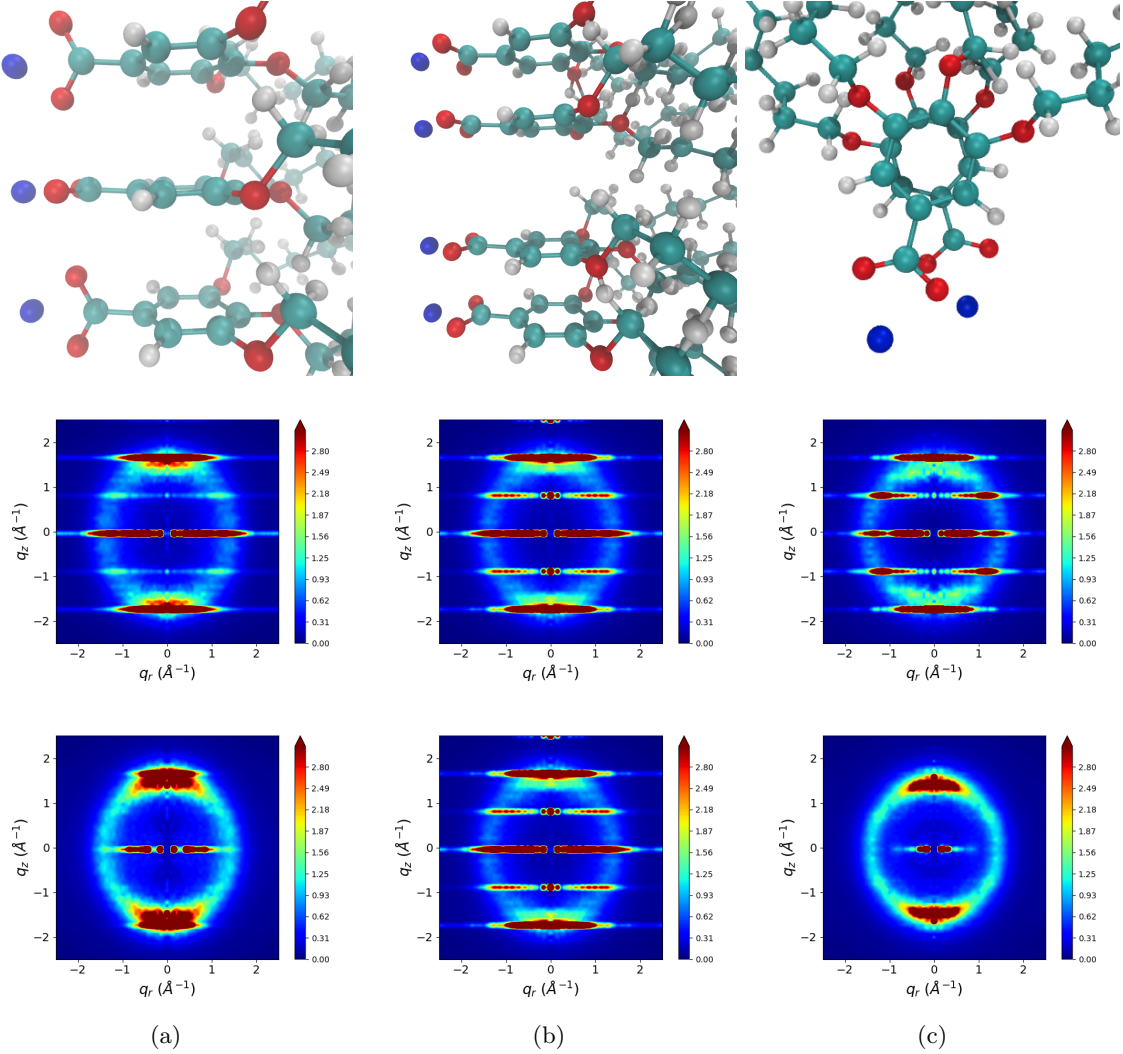


Figure 14: R-double is present in all three initial configurations tested while the heavy atoms in the headgroup are held in place with position restraints. R-double fades once the position restraints are released.

0.3 Pore composition

We plotted the number densities of heavy atoms in the head group, carbon atoms in the tail region and all sodium ions (Figure 15). For the head group region, we used the carbon atoms making up the aromatic ring. For the tail region we used only carbon atoms of the monomer tails (See Supporting Information for diagram). We average the histograms over at least 50 ns of equilibrated trajectory.

In general, the composition of the pores is similar between all systems.

- We believe we can study transport in any of the systems presented here and still extract valuable information.

- We will need to verify that this assumption is true.

In all cases, the space in the pore region is filled with sodium ions and head groups. Systems in the ordered pore basin are less dense in the center of the pore. In both the sandwiched and parallel displaced configurations, we see the density of head groups and sodium ions fall to less than 50% of its maximum at $r = 0$ (Fig. 15b). The situation is most pronounced in the sandwiched configuration where the maximum head group density occurs 0.44 nm from the pore center. The parallel displaced configuration reaches its maximum 0.35 nm from the pore center. In contrast, both disordered pore systems show very little difference in density from its maximum. This implies a more uniform distribution of head groups within the pore center. This is the same conclusion drawn from the plots of $g(x, y)$ (Figure ??).

There is a partition between the hydrophobic and hydrophilic regions, however it is a gradient in composition, rather than an abrupt division. The system does not confine sodium ions and head groups to just within the pore region. Assuming a pore radius of 0.6 nm, we see in all cases, that 19% of sodium ions exist outside the pore region (except sandwiched, ordered pore, where 16% are outside the pore). Additionally, we see that in all cases, about 3% of the plotted tail density is located within the pore region (except sandwiched, ordered pore, where 1.5% are within the pore region). These observations bring into question how one should define a pore in these types of systems. One usually measures a membrane's pore radius based on the size of a molecule it can reject, however it is not clear where the edges of the pores are and what size molecule would fit through. We leave these investigations for a future study.

END!!

Ionic conductivity calculation

We use the equilibrated parallel displaced system to calculate ionic conductivity since its structure is the closest match to experiment. The model gives reasonable estimates of ionic conductivity when compared to experiment.

- Calculated values of ionic conductivity obtained using the Nernst Einstein relation and Collective Diffusion model are compared in Figure 17.
- The two methods agree with each other within error, although the uncertainty obtained using the Collective Diffusion model is much higher.
- Much longer simulations are needed to lower the uncertainty, however it is not feasible to do so with a large system.
- For this reason we will likely only use the Nernst Einstein relation in future calculations of this type.

The calculated values of ionic conductivity are higher than experiment by an order of magnitude.

- One can justify the reason for this result by considering the real system studied experimentally
- The ionic conductivity measurement to which we are comparing was done on a 80 μm thick film, nearly 10,000 times thicker than our simulated system.
- The thick film likely has defects leading to non-contiguous pores and imperfect alignment.
- The 2D SAXS pattern shows the small degree of tortuosity present in the system (16)
- It has been shown that there is a large dependence of Ionic conductivity on the alignment of the pores
- The ionic conductivity of an unaligned film is 85 times lower than that of a nearly aligned film referenced here
- It is not unreasonable that a thin, perfectly aligned film would have a value of ionic conductivity in agreement with our model

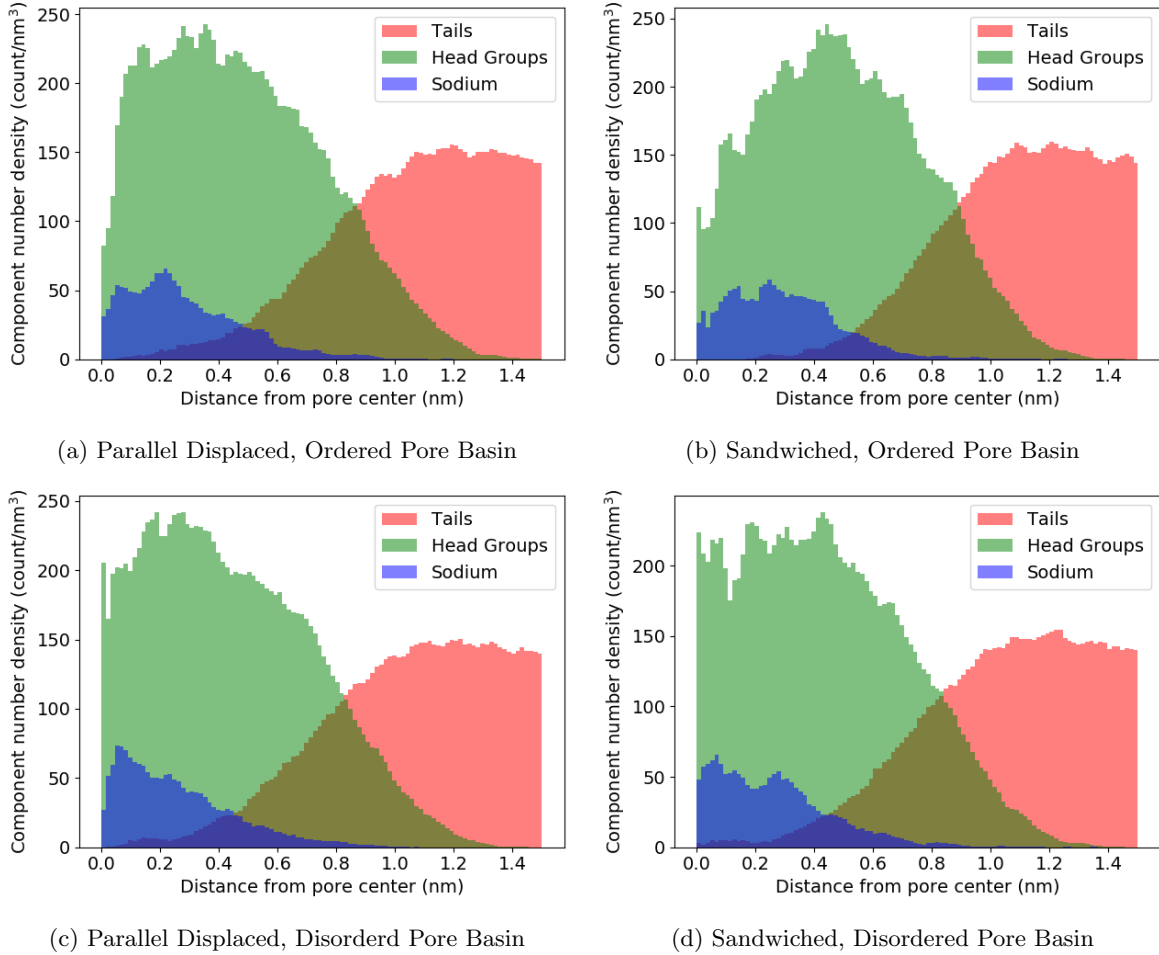


Figure 15: In all cases, the component radial distribution functions exhibit a composition gradient transitioning from the hydrophilic to the hydrophobic regions. Systems with layers initially spaced 3.7 Å apart in the parallel displaced (a), and sandwiched (b) configurations both show the highest concentrations of ions and head groups away from the pore center. Systems with layers initially spaced 5 Å apart (c) and (d), both show the highest concentrations of ions and head groups near the pore center, implying a more uniform, disordered pore.

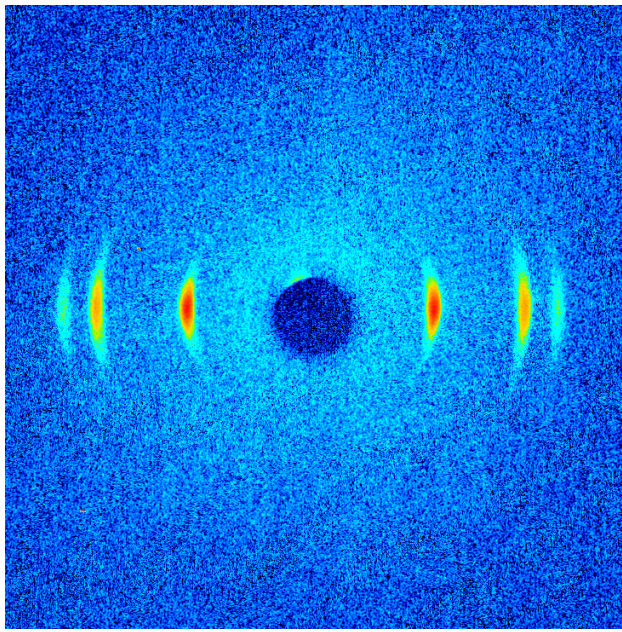


Figure 16: The experimental two dimensional SAXS pattern exhibits reflections resulting from highly aligned pore regions. A perfectly aligned system would exhibit sharp dots at the same locations of the refelctions shown. An isotropically aligned system the reflections would appear as rings centered about the origin

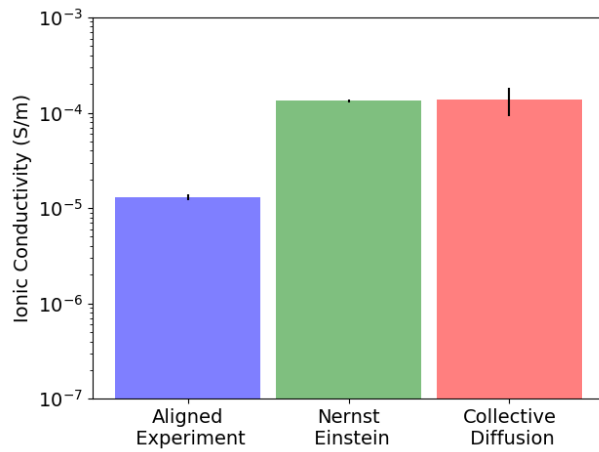


Figure 17: Calculated ionic conductivity using the Nernst-Einstein relation and Collective Diffusion model agree with error. Both methods give calculated values of ionic conductivity an order of magnitude higher than the experimental value

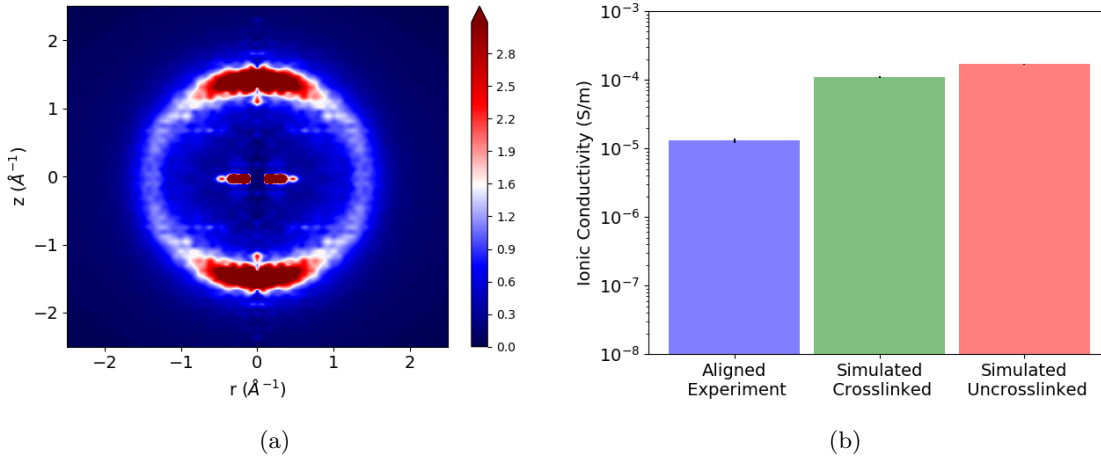


Figure 18: (a) Reflections produced by the crosslinked configuration fade relative to the uncrosslinked system. The colorbar shown is the same used for the uncrosslinked system. (b) The ionic conductivity is smaller relative to the uncrosslinked system, but still much larger than the experimental value

Implementation of the crosslinking algorithm

We applied the crosslinking algorithm to the equilibrated parallel-displaced configuration with 5 monomers per layer.

- We reach 95 % conversion of terminal vinyl groups
- The distance between pores shrinks by 0.4\AA after the system is crosslinked
- We simulated the crosslinked system in the NPT ensemble for 100 ns
- Major features are still present in the X-ray diffraction, however at lower intensities 18a
- The ionic conductivity is lower in the crosslinked system 18b

Conclusion

We have used a detailed molecular model of the Col_h phase formed by NA-GA3C11 in order to study the nanoscopic structure.

- While there have been efforts to model formation of various liquid crystalline phases with molecular dynamics, to our knowledge there have been no studies which attempt to examine their structure with the same level of detail presented here.
- Evidence strongly supports that layers are composed of 5 monomers
- We have confirmed that monomers stay partitioned in layers.
- We have explored the affect of two different $\pi-\pi$ stacking modes on the equilibrated membrane strucure.
- Simulated diffraction patterns generated from MD trajectories suggest that the parallel-displaced configuration produces a structure with the closest match to experiment.
- Finally, water is not needed to maintain membrane structure our data shows that it actually disorders the pore

- Now that we have a good idea of what the membrane structure should look like, we will evaluate transport of various solutes within the system.
- We will apply the knowledge gained from this study in order to suggest improvements to the existing system as well as to evaluate new unsynthesized LLC systems.

References

- [1] T. Humplik, J. Lee, S. C. OHern, B. A. Fellman, M. A. Baig, S. F. Hassan, M. A. Atieh, F. Rahman, T. Laoui, R. Karnik, and E. N. Wang, "Nanostructured materials for water desalination," *Nanotechnology*, vol. 22, no. 29, p. 292001, 2011.
- [2] B. Van Der Bruggen, C. Vandecasteele, T. Van Gestel, W. Doyen, and R. Leysen, "A review of pressure-driven membrane processes in wastewater treatment and drinking water production," *Environmental Progress*, vol. 22, pp. 46–56, Apr. 2003.
- [3] X. Song, Z. Liu, and D. D. Sun, "Nano Gives the Answer: Breaking the Bottleneck of Internal Concentration Polarization with a Nanofiber Composite Forward Osmosis Membrane for a High Water Production Rate," *Advanced Materials*, vol. 23, pp. 3256–3260, Aug. 2011.
- [4] R. L. McGinnis and M. Elimelech, "Global Challenges in Energy and Water Supply: The Promise of Engineered Osmosis," *Environmental Science & Technology*, vol. 42, pp. 8625–8629, Dec. 2008.
- [5] J. G. Wijmans and R. W. Baker, "The solution-diffusion model: a review," *Journal of Membrane Science*, vol. 107, pp. 1–21, Nov. 1995.
- [6] W. R. Bowen and J. S. Welfoot, "Modelling the performance of membrane nanofiltrationcritical assessment and model development," *Chemical Engineering Science*, vol. 57, pp. 1121–1137, Apr. 2002.
- [7] D. Cohen-Tanugi, L.-C. Lin, and J. Grossman, "Multilayer Nanoporous Graphene Membranes for Water Desalination," *Nano Letters*, vol. 16, pp. 1027–1033, Jan. 2016.
- [8] K. Hata, D. N. Futaba, K. Mizuno, T. Namai, M. Yumura, and S. Iijima, "Water-Assisted Highly Efficient Synthesis of Impurity-Free Single-Walled Carbon Nanotubes," *Science*, vol. 306, pp. 1362–1364, Nov. 2004.
- [9] S. Maruyama, E. Einarsson, Y. Murakami, and T. Edamura, "Growth process of vertically aligned single-walled carbon nanotubes," *Chemical Physics Letters*, vol. 403, pp. 320–323, Feb. 2005.
- [10] S. MURAD, K. ODER, and J. LIN, "Molecular simulation of osmosis, reverse osmosis, and electroosmosis in aqueous and methanolic electrolyte solutions," *Molecular Physics*, vol. 95, pp. 401–408, Oct. 1998.
- [11] L. Li, J. Dong, T. M. Nenoff, and R. Lee, "Desalination by reverse osmosis using MFI zeolite membranes," *Journal of Membrane Science*, vol. 243, pp. 401–404, Nov. 2004.
- [12] X. Feng, M. E. Tousley, M. G. Cowan, B. R. Wiesnauer, S. Nejati, Y. Choo, R. D. Noble, M. Elimelech, D. L. Gin, and C. O. Osuji, "Scalable Fabrication of Polymer Membranes with Vertically Aligned 1 nm Pores by Magnetic Field Directed Self-Assembly," *ACS Nano*, vol. 8, pp. 11977–11986, Dec. 2014.
- [13] R. C. Smith, W. M. Fischer, and D. L. Gin, "Ordered Poly(p-phenylenevinylene) Matrix Nanocomposites via Lyotropic Liquid-Crystalline Monomers," *Journal of the American Chemical Society*, vol. 119, no. 17, pp. 4092–4093, 1997.
- [14] M. Zhou, T. J. Kidd, R. D. Noble, and D. L. Gin, "Supported Lyotropic Liquid-Crystal Polymer Membranes: Promising Materials for Molecular-Size-Selective Aqueous Nanofiltration," *Advanced Materials*, vol. 17, pp. 1850–1853, Aug. 2005.
- [15] R. Resel, U. Theissl, C. Gadermaier, E. Zojer, M. Kriechbaum, H. Amenitsch, D. Gin, R. Smith, and G. Leising, "The H2-phase of the lyotropic liquid crystal sodium 3,4,5-tris(omega-acryloyloxyundecyloxy)benzoate," *Liquid Crystals*, vol. 27, pp. 407–411, Mar. 2000.
- [16] X. Feng, S. Nejati, M. G. Cowan, M. E. Tousley, B. R. Wiesnauer, R. D. Noble, M. Elimelech, D. L. Gin, and C. O. Osuji, "Thin Polymer Films with Continuous Vertically Aligned 1 nm Pores Fabricated by Soft Confinement," *ACS Nano*, vol. 10, pp. 150–158, Jan. 2016.

- [17] R. Resel, G. Leising, P. Markart, M. Kriechbaum, R. Smith, and D. Gin, “Structural properties of polymerised lyotropic liquid crystals phases of 3,4,5-tris(\$mega\$-acryloxyalkoxy)benzoate salts,” *Macromolecular Chemistry and Physics*, vol. 201, no. 11, pp. 1128–1133, 2000.
- [18] X. Zhu, M. Scherbina, A. Bakirov, B. Gorzolnik, S. Chvalun, U. Beginn, and M. Moller, “Methacrylated Self-Organizing 2,3,4-Tris(alkoxy)benzenesulfonate: A New Concept Toward Ion-Selective Membranes,” *ACS: Chemistry of Materials*, vol. 18, no. 19, pp. 4667–4673, 2006.
- [19] E. Gazit, “A possible role for -stacking in the self-assembly of amyloid fibrils,” *The FASEB Journal*, vol. 16, pp. 77–83, Jan. 2002.
- [20] M. O. Sinnokrot, E. F. Valeev, and C. D. Sherrill, “Estimates of the Ab Initio Limit for Interactions: The Benzene Dimer,” *Journal of the American Chemical Society*, vol. 124, pp. 10887–10893, Sept. 2002.
- [21] M. P. Waller, A. Robertazzi, J. A. Platts, D. E. Hibbs, and P. A. Williams, “Hybrid density functional theory for -stacking interactions: Application to benzenes, pyridines, and DNA bases,” *Journal of Computational Chemistry*, vol. 27, pp. 491–504, Mar. 2006.
- [22] A. L. Ringer, M. O. Sinnokrot, R. P. Lively, and C. D. Sherrill, “The Effect of Multiple Substituents on Sandwich and T-Shaped Interactions,” *Chemistry A European Journal*, vol. 12, pp. 3821–3828, May 2006.
- [23] J. Wang, R. M. Wolf, J. W. Caldwell, P. A. Kollman, and D. A. Case, “Development and testing of a general amber force field,” *Journal of Computational Chemistry*, vol. 25, pp. 1157–1174, July 2004.
- [24] J. Wang, W. Wang, P. A. Kollman, and D. A. Case, “Automatic atom type and bond type perception in molecular mechanical calculations,” *Journal of Molecular Graphics and Modelling*, vol. 25, pp. 247–260, Oct. 2006.
- [25] D. Case, R. Betz, W. Botello-Smith, D. Cerutti, T. Cheatham, III, T. Darden, R. Duke, T. Giese, H. Gohlke, A. Goetz, N. Homeyer, S. Izadi, P. Janowski, J. Kaus, A. Kovalenko, T. Lee, S. LeGrand, P. Li, C. Lin, T. Luchko, R. Luo, B. Madej, D. Mermelstein, K. Merz, G. Monard, H. Nguyen, H. Nguyen, I. Omelyan, A. Onufriev, D. Roe, A. Roitberg, C. Sagui, C. Simmerling, J. Swails, R. Walker, J. Wang, R. Wolf, X. Wu, L. Xiao, D. York, and P. Kollman, “AmberTools16,” Apr. 2016.
- [26] H. Bekker, H. J. C. Berendsen, E. J. Dijkstra, S. Achterop, R. van Drunen, D. van der Spoel, A. Si-jbers, H. Keegstra, B. Reitsma, and M. K. R. Renardus, “Gromacs: A parallel computer for molecular dynamics simulations,” *Physics Computing*, 1993.
- [27] H. J. C. Berendsen, D. van der Spoel, and R. van Drunen, “GROMACS: A message-passing parallel molecular dynamics implementation,” *Computer Physics Communications*, vol. 91, pp. 43–56, Sept. 1995.
- [28] D. Van Der Spoel, E. Lindahl, B. Hess, G. Groenhof, A. E. Mark, and H. J. C. Berendsen, “GROMACS: Fast, flexible, and free,” *Journal of Computational Chemistry*, vol. 26, pp. 1701–1718, Dec. 2005.
- [29] B. Hess, C. Kutzner, D. van der Spoel, and E. Lindahl, “GROMACS 4: Algorithms for Highly Efficient, Load-Balanced, and Scalable Molecular Simulation,” *Journal of Chemical Theory and Computation*, vol. 4, pp. 435–447, Mar. 2008.
- [30] J. Mondal, M. Mahanthappa, and A. Yethiraj, “Self-Assembly of Gemini Surfactants: A Computer Simulation Study,” *The Journal of Physical Chemistry B*, vol. 117, pp. 4254–4262, Apr. 2013.
- [31] L. Martnez, R. Andrade, E. G. Birgin, and J. M. Martnez, “PACKMOL: A package for building initial configurations for molecular dynamics simulations,” *Journal of Computational Chemistry*, vol. 30, pp. 2157–2164, Oct. 2009.
- [32] A. Einstein, “Investigations on the theory of the brownian movement,” *Dover Publications*, 1956.
- [33] Y. Liu and F. Zhu, “Collective diffusion model for ion conduction through microscopic channels,” *Biophysical Journal*, vol. 104, pp. 368–376, Jan. 2013.